Chinese Journal of Chemical Engineering 23 (2015) 31–41

Contents lists available at ScienceDirect

Chinese Journal of Chemical Engineering

journal homepage: www.elsevier.com/locate/CJCHE

Separation Science and Engineering

# Effect of sol size on nanofiltration performance of a sol–gel derived microporous zirconia membrane☆

Guizhi Zhu, Qian Jiang, Hong Qi *, Nanping Xu

*Membrane Science and Technology Research Center, State Key Laboratory of Materials-Oriented Chemical Engineering, Nanjing Tech University, Nanjing 210009, China*

ARTICLE INFO

*Article history:*
Received 18 March 2013
Received in revised form 3 December 2013
Accepted 30 December 2013
Available online 2 October 2014

*Keywords:*
Microporous ceramic membranes
Zirconia
Nanofiltration
Sol size
Sol–gel

ABSTRACT

This paper reports the effect of sol size on nanofiltration performances of sol–gel derived microporous zirconia membranes. Microstructure, pure water flux, molecular weight cut-off (MWCO) and salt retention of zirconia membranes derived from zirconia sols with different sizes were characterized. Thermal evolution, phase composition, microstructure and chemical stability of unsupported zirconia membranes (powder) were determined by thermogravimetric and differential thermal analysis, X-ray diffraction, nitrogen adsorption–desorption and static solubility measurements. Results show that nanofiltration performance of zirconia membranes is highly dependent on sol size. The sol with an average size of 3.8 nm, which is smaller than the pore size of the γ-$Al_2O_3$ support (pore size: 5–6 nm), forms a discontinuous zirconia separation layer because of excessive penetration of sol into the support. This zirconia membrane displays a MWCO value towards polyethylene glycol higher than 4000 Da. A smooth and defect-free zirconia membrane with a MWCO value of 1195 Da (pore size: 1.75 nm) and relative high retention rates towards $MgCl_2$ (76%) and $CaCl_2$ (64%) was successfully fabricated by dip-coating the sol with an appropriate size of 8.6 nm. Zirconia sol with an average size of 12 nm exhibits colloidal nature and forms a zirconia membrane with a MWCO value of 2332 Da (pore size: 2.47 nm). This promising microporous zirconia membrane presents sufficiently high chemical stability in a wide pH range of 1–12.


## 1. Introduction

Ceramic membranes have drawn a great deal of attention in the recent two decades because of their high chemical, thermal and mechanical stability in comparison with polymeric membranes. Ceramic membranes can be generally categorized into macroporous, mesoporous and microporous membranes based on the pore size [1]. In terms of the fabrication of macro- and mesoporous ceramic membranes, suspensions or colloidal sols are normally deposited onto the porous support, with subsequent sintering or calcination process. The pore structure is formed through particle packing and the relationship between the particle size of the starting material and the resulting pore size of the membrane can be quantitatively calculated [2]. Microporous ceramic membranes, including γ-$Al_2O_3$ [3], $SiO_2$ [4], $TiO_2$ [5], $ZrO_2$ [6] and $HfO_2$ [7], are hot topics in membrane research field in recent years, owing to their great potential applications in nanofiltration (NF), pervaporation (PV) and gas separation. Among them, $TiO_2$ and $ZrO_2$ are the most promising materials due to their high stability in harsh environments, especially long-term stability in a large pH range [1].

Polymeric sol–gel process is considered to be the most appropriate route for the fabrication of microporous ceramic membranes [1]. It is based on the chemistry of metal organic precursors in organic solvents. The first stage in the polymeric sol–gel process consists in the synthesis of a sol using molecular precursors (metal organics). Then the condensation reactions occur at the sol stage with the formation of polymeric clusters which interpenetrate with each other at the final stage to form the gel [8]. However, the extremely high hydrolysis and condensation rate of alkoxide precursors is one of the main hurdles for the synthesis of titania and/or zirconia polymeric sols and, further, quantitatively controls the sol size [9,10].

Table 1 summarizes the effect of sol size on the performance of microporous ceramic membranes. Polymeric hybrid $SiO_2$ sol presents an average size of 1.4 nm, which is much smaller than the pore size of the support, resulting in a discontinuous separation layer with a thickness less than 30 nm. The hybrid silica membrane fabricated by such sol exhibits a much lower separation factor of 8 for a mixture of *n*-butanol and water (95/5 , mass ratio) during PV processes [11]. On the other hand, a hybrid $SiO_2$ membrane fabricated with a polymeric

☆ Supported by the National Natural Science Foundation of China (20906047, 21276123), the National High Technology Research and Development Program of China (2012AA03A606), State Key Laboratory of Materials-Oriented Chemical Engineering (ZK201002), the Natural Science Research Plan of Jiangsu Universities (11KJB530006), the "Summit of the Six Top Talents" Program of Jiangsu Province, and a Project Funded by the Priority Academic Program development of Jiangsu Higher Education Institutions (PAPD).
* Corresponding author.
*E-mail address:* hqinjut@aliyun.com (H. Qi).

http://dx.doi.org/10.1016/j.cjche.2014.09.045
1004-9541/

**Table 1**
The effect of sol size on performance of microporous ceramic membranes

| Membrane material | Average sol size /nm | Support | Membrane thickness/nm (micrograph) | PV or NF performance | Reference |
|---|---|---|---|---|---|
| Hybrid $SiO_2$ | 1.4 | Tubular γ-$Al_2O_3$ (pore size: 5–6 nm) | 30 (not clear) | α = 8 | [11] |
| | 8 | | 120 (continuous and defect-free) | α = 300 | |
| | 13 | | >1000 (visible cracks) | – | |
| Hybrid $SiO_2$ | 3.3 | Tubular γ-$Al_2O_3$ (pore size: 4 nm) | 150 (continuous and defect-free) | α = 361 | [12] |
| | 5.7 | | 250 (continuous and defect-free) | α = 2695 | |
| $ZrO_2$ | 2 | Tubular γ-$Al_2O_3$ (pore size: 4 nm) | <10 (not clear) | – | [13] |
| | 3 | | 110 (many defects) | – | |
| | 10 | | ~150 (continuous and defect-free) | α = 171361 | |
| $ZrO_2$ | About 6 | Tubular γ-$Al_2O_3$ (pore size: 4 nm) | ~200 (clear) | No water permeation | [14] |
| | 5–10 | | 50 (clear) | MWCO < 300, pure water permeability: 0.256 $L\cdot m^{-2}\cdot h^{-1}\cdot MPa^{-1}$ | [15] |
| $TiO_2$ | 3 | Tubular γ-$Al_2O_3$ (pore size: 4 nm) | 20–30 | – | [13] |
| | 10 | | 150 (smooth and defect-free) | α = 171 361 | |
| $SiO_2$–$ZrO_2$ (mole ratio = 9:1) | 11 | Tubular $SiO_2$–$ZrO_2$ (pore size: 3 nm) | – | MWCO = 200 | [16] |
| | 13 | | – | MWCO = 500 | |
| | 16 | | – | MWCO = 1000 | |
| $ZrO_2$ | 3.8 | Disk γ-$Al_2O_3$ (pore size: 5–6 nm) | (Discontinuous) | MWCO > 4000 | This work |
| | 8.6 | | (Smooth, continuous and defect-free) | MWCO = 1195 | |
| | 12 | | (Continuous and defect-free) | MWCO = 2332 | |

α: separation factor towards a mixture of *n*-butanol and water (95/5, mass ratio) operated at 95 °C (PV performance).

sol size of 13 nm, which is larger than the pore size of the support, exhibits visible cracks [11]. This phenomenon can be attributed to the fact that the membrane thickness is larger than the critical value. A microporous $SiO_2$-based membrane, fabricated by dip-coating a hybrid $SiO_2$ sol with an average size of 8 nm, gives a separation factor (α) of 300 for a mixture of *n*-butanol and water (95/5, mass ratio) during PV process [11]. It is also reported that a hybrid $SiO_2$ sol with an average size of 5–6 nm is suitable for fabrication of $SiO_2$-based membranes [12,17–19]. Although the relationship between silica-based sol size and PV performance of microporous $SiO_2$ membranes is clear, few silica-based NF membranes are reported due to its chemical instability in extreme pH environments. In comparison with $SiO_2$-based materials, $TiO_2$ and $ZrO_2$ materials exhibit much higher chemical stability and, hence, much research work is focused on the development of $TiO_2$ and $ZrO_2$ NF membranes [1]. These NF membranes hold great promise for the separation and purification of catalyst [20], dyes [21], and heavy mental ions [22,23] *via* the charging mechanism and sieving effect. However, the investigation on the relationship between titania and/or zirconia sol size and NF performance of those membranes is scarce. More importantly, appropriate sol size for fabrication of $TiO_2$ and/or $ZrO_2$ nanofiltration membrane is still ambiguous. As can be seen in Table 1, a zirconia membrane derived from a zirconia sol with an average size of 2–3 nm shows a discontinuous separation layer with many defects [13]. A dense zirconia membrane fabricated by using the sol with a size of about 6 nm cannot permeate water even under a trans-membrane pressure as high as 1.0 MPa [14]. It is also reported that a zirconia nanofiltration membrane, fabricated by dip-coating zirconia sol with particle size in the range of 5–10 nm, presents a MWCO < 300 and a pure water flux of 0.256 $L\cdot m^{-2}\cdot h^{-1}\cdot MPa^{-1}$ [15]. Therefore, more information on the effect of sol size on nanofiltration performance of zirconia membranes is urgently needed. Such investigation will guide the fabrication of zirconia nanofiltration membranes.

In previous work [24], we synthesized stable zirconia polymeric sols with the average sizes in the range of 1–12 nm and investigated the effects of the processing parameters (*e.g.* hydrolysis time, hydrolysis temperature, hydrolysis ratio and doping of chelating agent) on the state and average size of $ZrO_2$ sols. The aim of this work is to systematically investigate the effect of sol size on NF performance of microporous zirconia membranes. High quality supported mesoporous γ-$Al_2O_3$ layer with controlled pore size (5–6 nm) is used as the support for dip-coating. Microstructure, pure water flux, molecular weight cut-off (MWCO) and salt retention of zirconia membranes from zirconia sols with different sizes are characterized. The properties of unsupported zirconia membranes (powder) are also determined by XRD, TG/DTA, nitrogen adsorption–desorption and static solubility measurements.

## 2. Experimental

### 2.1. Synthesis of $ZrO_2$ sols and fabrication of $ZrO_2$ membranes

Zirconia sols were synthesized through polymeric sol–gel route by using zirconium *n*-propoxide (70% in propanol, ABCR GmbH & Co., denoted as ZnP) as a precursor and diethanolamine (DEA, Shanghai Lingfeng Chemical Reagent Co.) as a chelating agent. Recipes for the synthesis of $ZrO_2$ sols are displayed in Table 2. The general procedure for the preparation of a $ZrO_2$ sol is as follows. 4.5 ml ZnP was added into 20 ml 1-propanol (Shanghai Lingfeng Chemical Reagent Co.), and then a certain quantity of DEA was drop-wise introduced into the ZnP solution under vigorous stirring. Both operations were carried out in a nitrogen glove box. The mixture was immediately placed into an ice bath to prevent premature hydrolysis. Deionized water was drop-wise added into the solution under vigorous stirring and subsequently maintained at a fixed temperature for a certain period of time. The obtained $ZrO_2$ sols (referred to as DZ sols) were cooled down to room temperature and diluted 6 times with 1-propanol before dip-coating. Dip-coating is the most commonly used method for the formation of a membrane layer on porous supports. With a disk support withdrawn from a sol in a well-defined manner, a wet layer covering the substrate can be obtained either through capillary filtration or film-coating mechanism. In this study, supported $ZrO_2$ membranes were fabricated

**Table 2**
Recipes for the synthesis of $ZrO_2$ sols

| Sol number | Hydrolysis temperature/°C | Hydrolysis time/min | $[H_2O]/[ZnP]$ (molar ratio) | [DEA]/[ZnP] (molar ratio) | Particle size distribution/nm | Viscosity/Pa·s |
|---|---|---|---|---|---|---|
| DZ-1 | 0 | 12 | 5.0 | 2.2 | 2.7–15.2 | $3.02 \times 10^{-3}$ |
| DZ-2 | 40 | 180 | 9.4 | 2.2 | 5.4–21.5 | $3.10 \times 10^{-3}$ |
| DZ-3 | 40 | 180 | 9.4 | 1.3 | 7.6–51.1 | $3.32 \times 10^{-3}$ |

through dip-coating the DZ sols onto home-made disk α-alumina supported mesoporous γ-alumina layers (pore size: 5–6 nm) under clean room (class 1000) conditions. Then $ZrO_2$ membranes were calcined under air at 400 °C for 3 h (denoted as DZ membranes) with the heating and cooling rates of 0.5 °C·min$^{-1}$. Zirconia powder (designated as DZ powder) was obtained by drying corresponding DZ sols in a Petri dish overnight, followed by calcination procedures the same as that for supported DZ membranes.

### 2.2. Characterization of sols and membranes

Effective particle sizes in the $ZrO_2$ sols were measured by Dynamic Light Scattering using a Zetatrac analyzer (Microtrac Inc.). The average hydrodynamic diameters of DZ sols reported in this study are the volume weighted mean diameter derived from a cumulant analysis in the Microtrac software. The viscosities of polymeric $ZrO_2$ sols were measured by rotary viscosimeter (DVIII+, Brookfield) at 30 °C. Phase compositions of DZ powder were evaluated by employing X-ray diffraction (XRD, Bruker D8, Advance diffractometer), using a target of Cu $K_a$ operated at 40 kV and 40 mA. Thermal evolution of DZ powder was measured using a combined thermogravimetry and differential thermal analysis (TG/DTA) apparatus (STA-449-F3, Netzsch) under oxygen with a heating rate of 10 °C·min$^{-1}$ in the temperature range of 40–1000 °C. Nitrogen adsorption measurements were conducted at 77 K on Belsorp-mini (Bel Inc.) instruments. Prior to measurements, all samples were vacuum-dried at 200 °C for 3 h. Microstructure of DZ membranes was observed by field emission scanning electron microscopy (FESEM, Carl Zeiss, Leo 1550).

The chemical stability of microporous zirconia membranes, represented by the corrosion-resistant property of corresponding zirconia powder, was determined by using static solubility test of zirconia powder [25], with the general procedure as follows. 100 mg of zirconia powder was immersed in a 100 ml solution, whose pH value (1–12) was adjusted by the addition of nitric acid or sodium hydroxide. The solution was kept stirring for 4 days in a polytetrafluoroethylene beaker by using a magnetic stirrer before it was filtered over a qualitative filter paper with a pore size of 1–3 μm. The concentration of Zr ion in the solution was determined by inductively coupled plasma optical emission spectrometry (ICP, 7000 DV, PE).

Pure water flux of disk membranes was characterized by using a dead-end filtration apparatus [24] under trans-membrane pressures in the range of 0.3–0.7 MPa. Polyethylene glycol (PEG) retention of $ZrO_2$ membrane (DZ membrane) was characterized by using the same apparatus with the feed solution stirring at a speed of 200 r·min$^{-1}$ to avoid concentration gradient. The feed solution contained PEGs (Alfa Aesar) with molecular masses of 200, 600, 1500 and 4000, with the overall concentration of 3 g·L$^{-1}$ (with each PEG in 0.75 g·L$^{-1}$). The measurement was conducted at a trans-membrane pressure of 0.76 MPa and a temperature of (25 ± 2) °C. The retention rate of the membrane was determined with gel permeation chromatography (GPC, Waters), by collecting both feed and permeate solutions. The molecular mass of PEG corresponding to a 90% retention level was taken as the MWCO of DZ membranes. Salt retention of $ZrO_2$ membranes with respect to single component salt solutions, such as $MgCl_2$, $CaCl_2$, $Na_2SO_4$ and NaCl, was determined by using the same filtration apparatus under trans-membrane pressures in the range of 0.4–0.8 MPa at ambient temperature (25 ± 2) °C. The feed solution was kept stirring at a speed of 200 r·min$^{-1}$ to avoid concentration gradient. The concentration and pH value of above-mentioned salt solutions were controlled in the range of 0.005–0.1 mol·L$^{-1}$ and 6.0 (adjusted by addition of $HNO_3$ or $NH_3 \cdot H_2O$), respectively. Salt retention of $ZrO_2$ membrane was determined by measuring conductivities of salt solutions using conductivity meter (DDS-307, Shanghai Leici Instrument Factory), which are collected from both feed and permeate sides.

## 3. Results and Discussion

### 3.1. Particle size distributions of zirconia sols and stability

Particle size distributions (PSDs) of freshly prepared DZ sols and the sols stored at −20 °C for 3 months are displayed in Fig. 1. All freshly prepared zirconia sols exhibit uni-modal distributions, with mode particle sizes of 3.8, 8.6 and 12 nm, while the appearances of DZ-1–DZ-3 sols are clear and transparent. The PSDs as well as the viscosities of DZ sols are shown in Table 2, among which DZ-3 sol displays a much boarder PSD in the range of 7.6–51.1 nm and a relative high viscosity of 3.32 ×10$^{-3}$Pa·s It indicates the occurrence of higher hydrolysis and condensation reaction, which might lead to the formation of highly

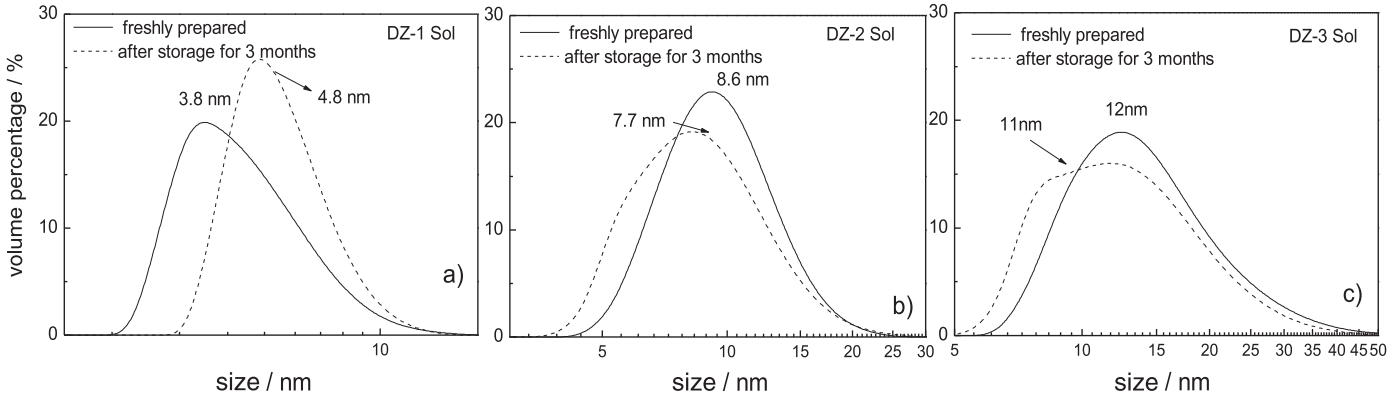


**Fig. 1.** Particle size distributions of freshly prepared $ZrO_2$ sols and those stored at −20 °C for 3 months. (a) DZ-1 sol; (b) DZ-2 sol; (c) DZ-3 sol.

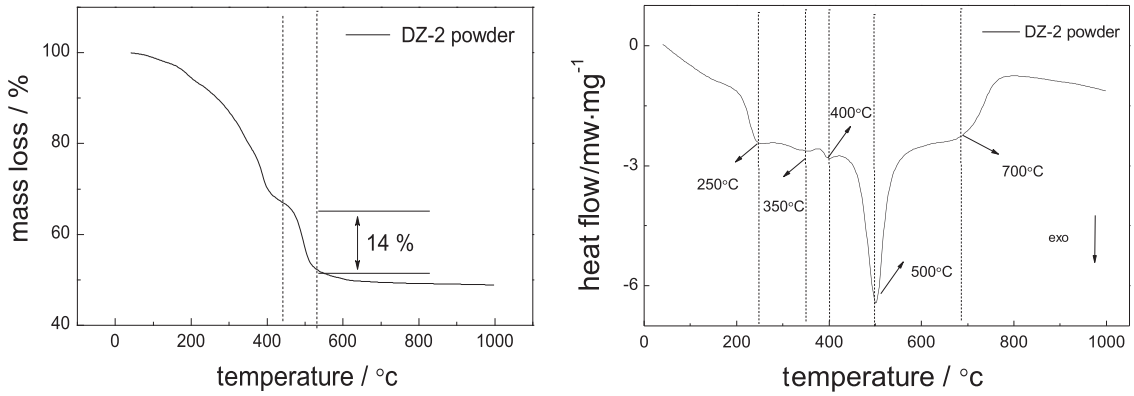


**Fig. 2.** Thermogravimetric and differential thermal analysis curves of DZ-2 powder.

branched cluster in the sol. The variation of the viscosity, on the other hand, confirms the inhabitation effect of the addition of DEA on the hydrolysis and condensation of zirconium alkoxide precursor. The stabilities of the sols characterized by its variation of the PSD after storage for a period of time are also shown in Fig. 1. After 3 months of storage at −20 °C, the minimum size of DZ-1 sol shifts to ~3 nm while the maximum size keeps unchanged. It may be resulted from the continuous polymerization in the DZ-1 sol during the storage. However, the minimum and maximum sizes of DZ-2 and DZ-3 sols change little after 3 months of storage. More importantly, the mode sizes of DZ-2 (7.7 nm) and DZ-3 (11 nm) sols do not vary much after storage. It indicates good stabilities of DZ-2 and DZ-3 sols. Meanwhile, the appearances of all DZ sols remain clear and transparent, which is one of the prerequisites for the fabrication of microporous membranes.

### *3.2. Properties of unsupported DZ membranes (DZ powder) derived from zirconia sols*

Since the DZ powder presents similar behavior in the heat-treating process irrespective of the sol size, thermogravimetric and differential thermal analyses of DZ-2 powder are shown in Fig. 2. An initial mass decrease prior to 250 °C in the TG curve can be attributed to the removal of physically adsorbed water and solvent. The decomposition of alkoxide should be responsible for the exothermic peak at around 250 °C in the DTA curve. Similar result has been observed by Aust *et al.* [26]. A small exothermic peak at around 350 °C in the DTA curve can be attributed to the removal of unreacted chelating agent DEA, whose boiling temperature is at 271 °C. The exothermic peak at around 400 °C in the DTA curve is attributed to the phase transformation of zirconia powder from amorphous to tetragonal. A sharp mass loss (approximately 14%) started from 440 °C and ended at around 560 °C, together with a large exothermic peak near 500 °C in the DTA curve, may be due to the removal of chelated zirconium complex inside the material [27,28]. The exothermic peak at around 700 °C in the DTA curve is attributed to the phase transformation of zirconia powder from tetragonal to monoclinic [29].

To probe the phase evolution of DZ powder derived from zirconia sols with different sizes, XRD measurements were conducted on DZ powder calcined at different temperatures, and the results are shown in Fig. 3. The DZ powder presents similar phase compositions at the same calcination temperature irrespective of the sol size. The DZ powder exhibits amorphous nature up to a calcination temperature of 350 °C, while the tetragonal phase can be detected for all 400 °C-calcined DZ powder. It should be noted, however, that the peak intensity of tetragonal phase increases as the calcination temperature elevates from 400 °C to 500 °C. It has been reported that the phase transition of oxide is normally accompanied with considerable grain growth and pore enlargement [30,31]. Our previous research has also found that the MWCO value of zirconia membrane increases with calcination temperature, from 354 Da (350 °C) to 1195 Da (400 °C) [24].

It is well known that microporous materials present type I sorption isothermal characteristic and hold large $V_{micro}/V_{total}$ ratio [32,33]. Nitrogen adsorption–desorption isotherms of DZ powder are shown in Fig. 4. All isotherms of DZ powder calcined at 400 °C present type I curve irrespective of the sol size, indicating the formation of microporous structures. Pore structures of DZ powder calcined at 400 °C are displayed in Table 3, in which the specific surface areas are derived from the Brunauer, Emmet and Teller (BET) theory. The microporous and total volumes are obtained by recording the adsorbed volume ($V_a$) of powder at $P/P_0 = 0.1$ and $P/P_0 = 0.95$ [32]. It can be seen in Table 3 that $V_{micro}/V_{total}$ ratio of DZ powder decreases with the increase

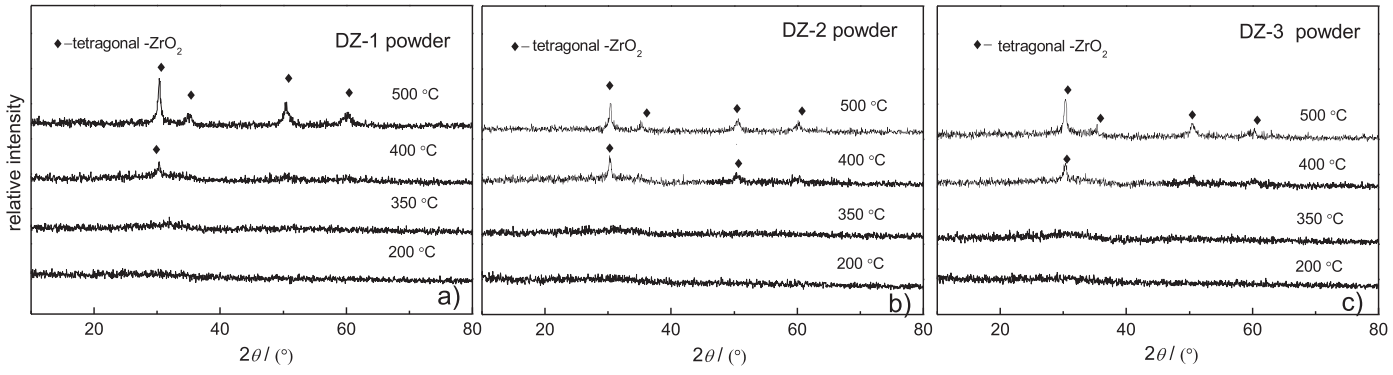


**Fig. 3.** XRD patterns of DZ powder calcined at different temperatures. (a) DZ-1; (b) DZ-2; (c) DZ-3.

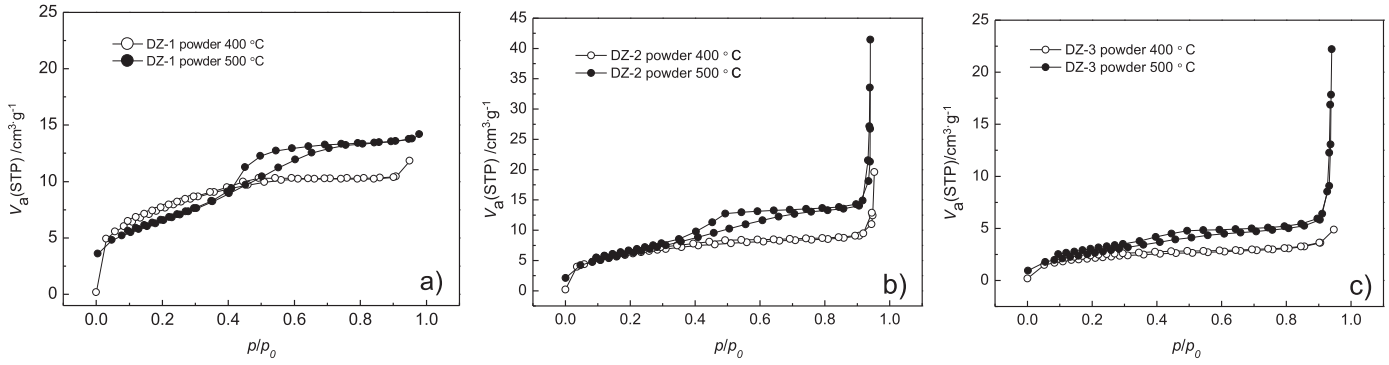


**Fig. 4.** Nitrogen adsorption–desorption isotherms of DZ powder calcined at 400 °C. (a) DZ-1; (b) DZ-2; (c) DZ-3.

**Table 3**
Properties of $ZrO_2$ powder calcined at 400 °C

| Sample | BET surface area/m$^2$·g$^{-1}$ | $V_{total}$ (STP)/cm$^3$·g$^{-1}$ | $V_{micro}$ (STP)/cm$^3$·g$^{-1}$ | $V_{micro}/V_{total}$/% |
|---|---|---|---|---|
| DZ-1 (400) | 18.29 | 11.84 | 6.4 | 54.05 |
| DZ-2 (400) | 14.04 | 11.01 | 5.09 | 46.23 |
| DZ-3 (400) | 4.82 | 4.89 | 1.83 | 37.42 |

STP: standard temperature and pressure; $V_{total} = V_a$ at $P/P_0 = 0.95$; $V_{micro} = V_a$ at $P/P_0 = 0.1$.

of sol size, from 54.05% (DZ-1 powder derived from zirconia sol with an average size of 3.8 nm) to 37.42% (DZ-3 powder derived from zirconia sol with an average size of 12 nm), indicating that the increase of sol size results in the transformation of the powder from a majority of microporous structure to a minority one. The values of $V_{total}$ and $V_{micro}$ do not vary much when the sol size is smaller than 8.6 nm, while decreases sharply when the sol size reaches 12 nm. It has been reported that BET surface area of microporous powder in colloidal nature decreases with increasing sol size, while the tendency is opposite for polymeric microstructures [5]. The slight variation of BET surface area, from 18.29 m$^2$·g$^{-1}$ to 14.04 m$^2$·g$^{-1}$, shows that the powder from zirconia sol with an average size smaller than 8.6 nm retains polymeric microstructures. The sharp decrease of BET surface area, from 14.04 m$^2$·g$^{-1}$ to 4.82 m$^2$·g$^{-1}$, indicates that the powder with 12 nm-sized sol forms preferred colloidal microstructure. When the calcination temperature reaches 500 °C, all isotherms of DZ powder show a hysteretic loop (*i.e.* type IV sorption isotherm), indicating the formation of mesoporous structures.

Thus the increase of sol size, from 3.8 nm to 12 nm, not only increases porous volume, but also forms preferred microporous structure from polymeric to colloidal nature, which would affect the properties of membranes derived from corresponding zirconia sols. Taking into account that the increase of calcination temperature may result in the phase transformation accompanied with volume variation and pore growth, which might cause cracks and/or defects in the membrane [34], the calcination temperature of the zirconia membrane below was set at 400 °C.

### 3.3. Microstructures of DZ membranes

Figs. 5 and 6 give the cross-section and surface photos of DZ-1 membrane, derived from a sol with an average size of 3.8 nm. A rather thin (less than 100 nm) top layer forms on the γ-$Al_2O_3$ support with the sol deposited, while a rough surface with many large defects can be observed in the membrane (Fig. 6). Considering the relative small size of DZ-1 sol (3.8 nm) as compared with the pore size of γ-$Al_2O_3$ support (5–6 nm), it is believed that a discontinuous zirconia separation layer forms due to excessive penetration of DZ-1 sol into the support. The microstructures of DZ-2 membrane are shown in Figs. 7 and 8. A thick top layer (*ca.* 100 nm) can be observed in DZ-2 membrane fabricated with a sol with an average size of 8.6 nm. It should be noted that DZ-2 membrane presents smooth and defect-free surface, as evidenced in Fig. 8. In comparison with DZ-1 membrane, the improvement of the quality of top layer of DZ-2 membrane can be assigned to the increase of sol size from 3.8 nm to 8.6 nm, successfully preventing the sol from intensive intrusion into the γ-$Al_2O_3$ support and eventually giving

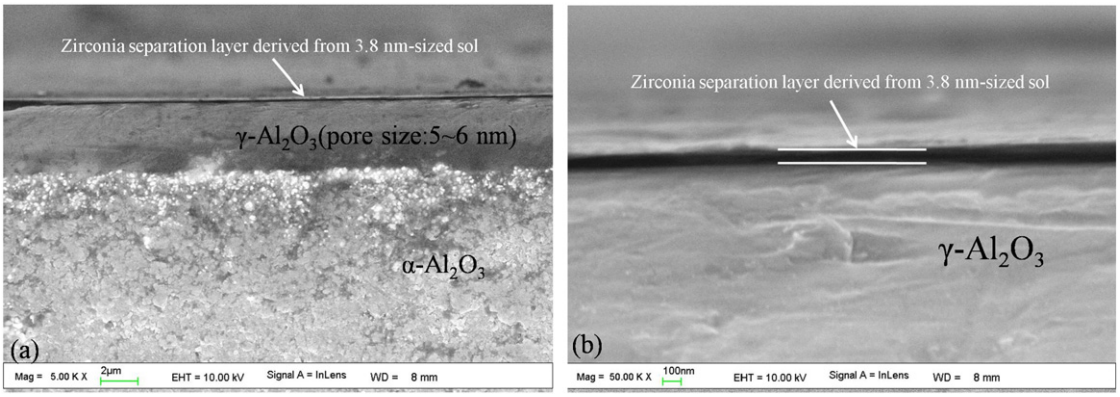


**Fig. 5.** FESEM photos of the cross-section of DZ-1 membrane derived from a sol with an average size of 3.8 nm. (a) Bar = 2 μm; (b) Bar = 100 nm.

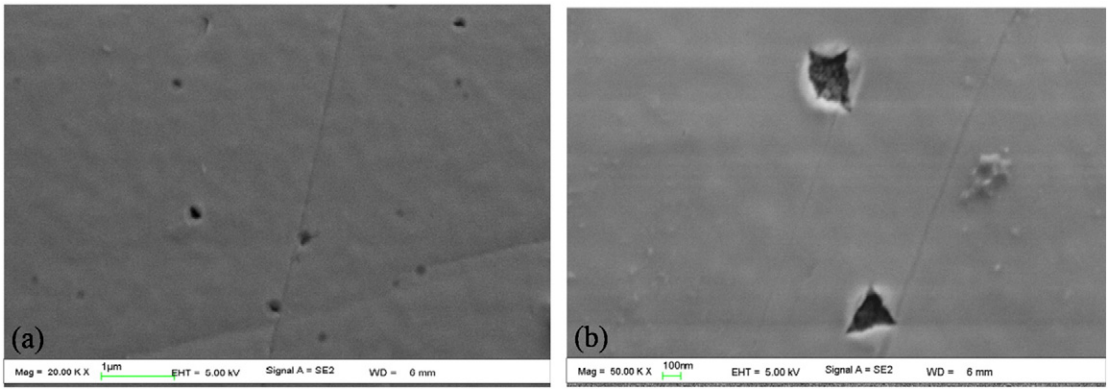


**Fig. 6.** FESEM photos of the surface of DZ-1 membrane derived from a sol with an average size of 3.8 nm. (a) Bar = 1 μm; (b) Bar = 100 nm.

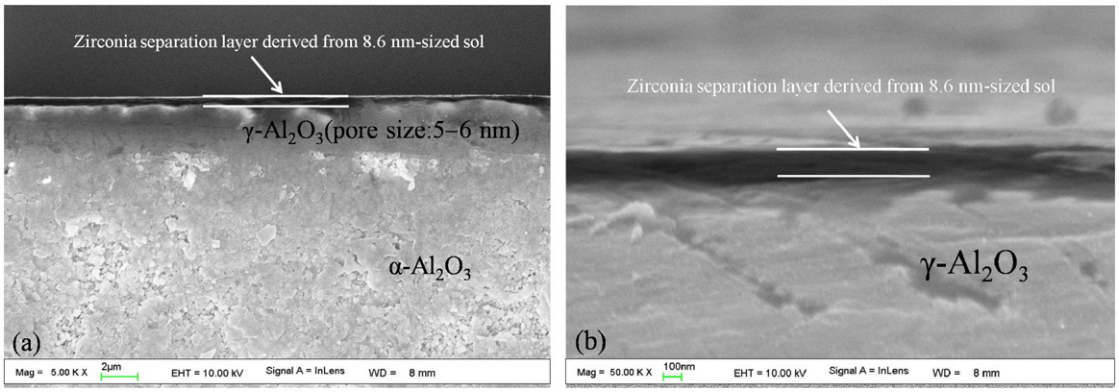


**Fig. 7.** FESEM photos of the cross-section of DZ-2 membrane derived from a sol with an average size of 8.6 nm. (a) Bar = 2 μm; (b) Bar = 100 nm.

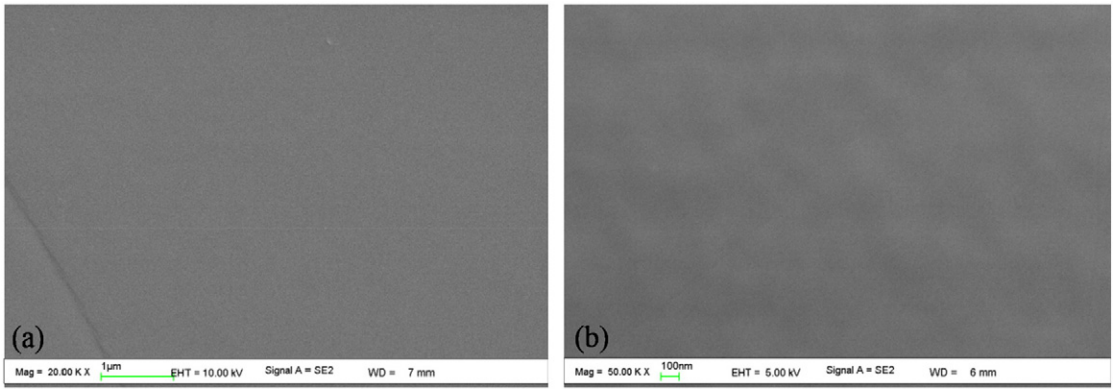


**Fig. 8.** FESEM photos of the surface of DZ-2 membrane derived from a sol with an average size of 8.6 nm. (a) Bar = 1 μm; (b) Bar = 100 nm.

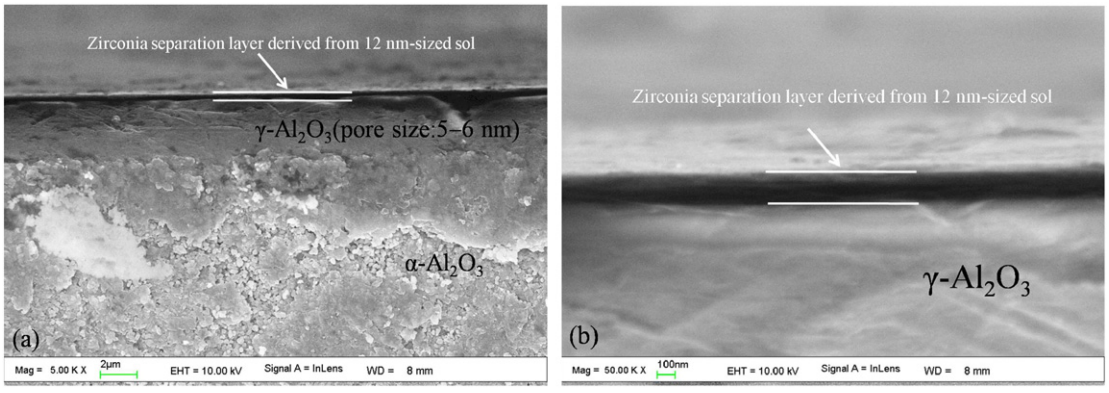


**Fig. 9.** FESEM photos of the cross-section of DZ-3 membrane derived from a sol with an average size of 12 nm. (a) Bar = 2 μm; (b) Bar = 100 nm.

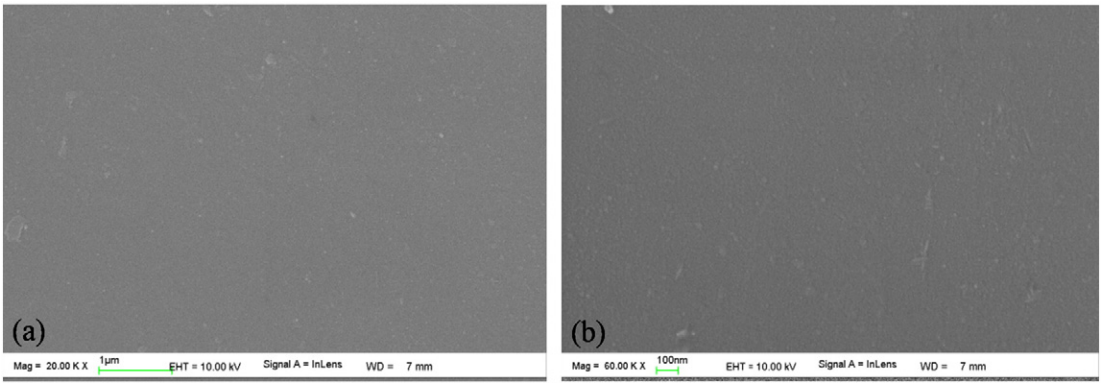


**Fig. 10.** FESEM photos of the surface of DZ-3 membrane derived from a sol with an average size of 12 nm. Bar = 1 μm; (b) Bar = 100 nm.

a defect-free and homogeneous zirconia separation layer. Figs. 9 and 10 give FESEM photos of cross-section and surface of DZ-3 membrane, derived from the sol with an average size of 12 nm. As can be seen in Fig. 9, DZ-3 membrane shows similar cross-section micrograph (with a thickness of ~200 nm) to that of DZ-2 membrane, indicating that membrane deposited by DZ-3 sol with an average size of 12 nm could also successfully prevent excessive penetration of the sol into the γ-$Al_2O_3$ support. Fig. 10 shows a smooth surface with a few irregular dots in DZ-3 membrane.

Based on these results, we can conclude that for a specific support, the sol size will inevitably affect the microstructure of sol–gel derived membranes. Zirconia sol with a size larger than the pore size of γ-$Al_2O_3$ support could efficiently prevent from intensive penetration into the support and, hence, lead to a defect-free and homogeneous separation layer.

### *3.4. Effect of sol size on nanofiltration performance of microporous zirconia membranes*

PEG retention of $ZrO_2$ membranes calcined at 400 °C is shown in Fig. 11. DZ membranes derived from zirconia sols with different PSDs display various retention performance towards PEGs. Although DZ-1 powder calcined at 400 °C shows a majority of microporous structure, DZ-1 membrane shows only a 70% retention rate towards PEG with a molecular weight of 4000, indicating that the pore size of the membrane is too large to reject organic substance efficiently. The defects formed on membrane surface as shown in Fig. 6 also corroborate the low PEGs retention of DZ-1 membrane. The sol with an average size smaller than the pore size of support would cause excessive penetration into the support and, eventually, lead to the formation of a discontinuous zirconia separation layer. DZ-2 membrane fabricated by DZ-2 sol with an average size of 8.6 nm exhibits a MWCO value of 1195, corresponding to a pore size of 1.75 nm based on the calculation as follows [35]:

$$R = \left(0.262 \times {M_W}^{0.5} - 0.3\right) \times 0.1 \quad (1)$$

where $R$ (nm) is the pore radius of membrane and $M_W$ is the MWCO.

The result indicates successful deposition of a defect-free and continuous separation layer onto the γ-$Al_2O_3$ support, with pore size (5–6 nm) slightly smaller than the average size of deposited DZ-2 sol. Hence, the average size of DZ-2 sol (8.6 nm) is considered to be large enough to prevent from intensive intrusion into the γ-$Al_2O_3$ support. More importantly, the result also demonstrates that DZ-2 sol retains a polymeric nature, allows interpenetration of polymer chains and, thus, results in the formation of microporous structures. The results line up with those observations made by Vacassy *et al.* [36] and Xu and Anderson [37], who reported that sol with an average size less than 10 nm is suitable for the fabrication of microporous membranes. The observation is also consistent with the data obtained from nitrogen adsorption–desorption curves and FESEM images of DZ-2 membrane displayed in Figs. 4, 7 and 8. As can be seen from Figs. 7–10, DZ-3 membrane shows similar microstructures to that in DZ-2 membrane. However, DZ-3 membrane presents a higher MWCO value of 2332 (corresponding to a pore size of 2.47 nm as calculated by Eq. (1)) in comparison with DZ-2 membrane. Larger pore size of DZ-3 membrane can be attributed to the fact that a highly branched cluster and/or sol with colloidal nature are formed in DZ-3 sol, as evidenced by the sol size, nitrogen adsorption–desorption curves and FESEM images in Figs. 1, 4 and 10, respectively. These results are also consistent with a minority of microporous structure of the 400 °C-calcined DZ-3 powder. Consequently,

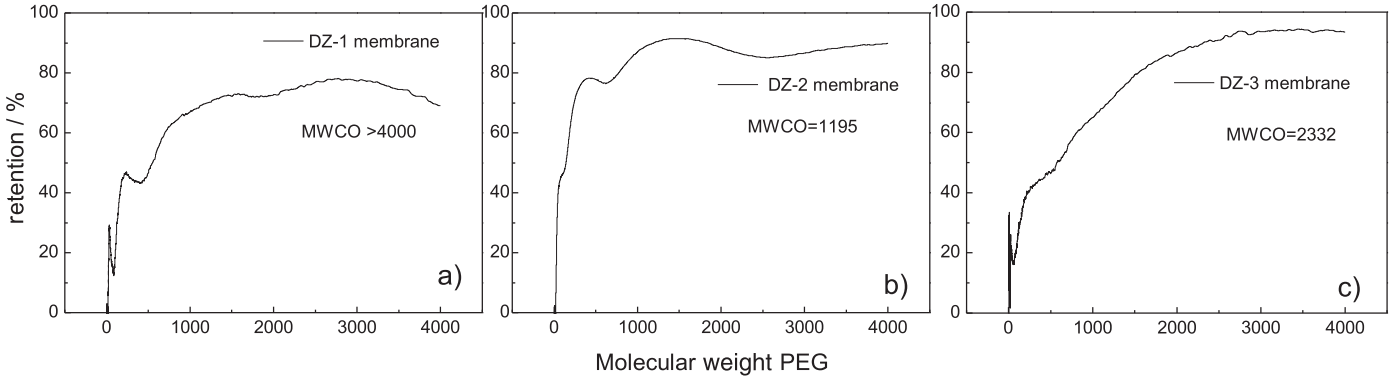


**Fig. 11.** PEG retention of $ZrO_2$ membranes calcined at 400 °C. (a) DZ-1; (b) DZ-2; (c) DZ-3.

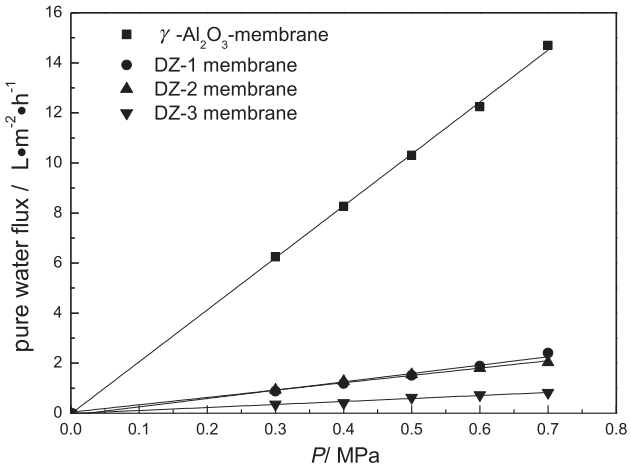


**Fig. 12.** Pure water flux of zirconia membranes calcined at 400 °C and γ-$Al_2O_3$ support.

the sol size is relative to the nature of the sol and, hence, affects the performance of membranes. A low branched zirconia sol is preferable to fabricate microporous zirconia membranes by tuning the average sol size smaller than 12 nm.

The pure water flux of γ-$Al_2O_3$ support and three DZ membranes are depicted in Fig. 12. The pure water flux of all membranes increases linearly with the trans-membrane pressure, with pure water flux of 0.2,0.033,0.029 and 0.012 $L \cdot m^{-2} \cdot h^{-1} \cdot MPa^{-1}$, respectively. It is well known that the membrane permeability is inversely proportional to the membrane thickness [30]. Taking into account that the thickness of DZ membranes are less than 100 nm, about 100 and 200 nm (as shown in Figs. 5–10), the pure water flux of DZ membranes in the sequence of *F*(DZ-1) > *F*(DZ-2) > *F*(DZ-3) is reasonable. The sharply decreased pure water flux is another evidence for the formation of defect-free and continuous top zirconia layers on the γ-$Al_2O_3$ support.

Ionic retention of DZ membranes towards single component salt solutions of $CaCl_2$, $MgCl_2$, NaCl and $Na_2SO_4$ is displayed in Fig. 13. All ionic retention rates decrease as salt concentration increases, which can be explained by the reduction of thickness of the double electronic layer formed in the membrane pores [38,39]. With the increase of salt concentration (*i.e.* higher ionic strength), the thickness of the double electronic layer decreases, which is responsible for the lower retention rates of DZ membranes. The ion rejection of nanofiltration membrane is determined by the charging effects and sieving effects [40]. Since the hydrated radius of cations in this study is much smaller than that of the $ZrO_2$ membrane, the ion retention is primarily influenced by the membrane charging effects [39]. The repulsive force between the membrane and di-valent co-ions is stronger than that with monovalent co-ions. This would lead to the retention sequence of *R*($CaCl_2$, $MgCl_2$) > *R*(NaCl, $Na_2SO_4$) [3,39]. The DZ-1 membrane fabricated by a sol with an average size of 3.8 nm, which is slightly smaller than the pore size of γ-$Al_2O_3$ support, shows a relative lower retention property towards 0.005 $mol \cdot L^{-1}$ di-valent salt solutions, as evidenced by the retention rates of 56% ($CaCl_2$) and 53% ($MgCl_2$). The relatively lower ionic retention is another evidence for the formation of a discontinuous zirconia separation layer on the γ-$Al_2O_3$ support because of excessive penetration of DZ-1 sol into the mesoporous support, which favors transport of ions through large pores. DZ-2 and DZ-3 membranes derived from

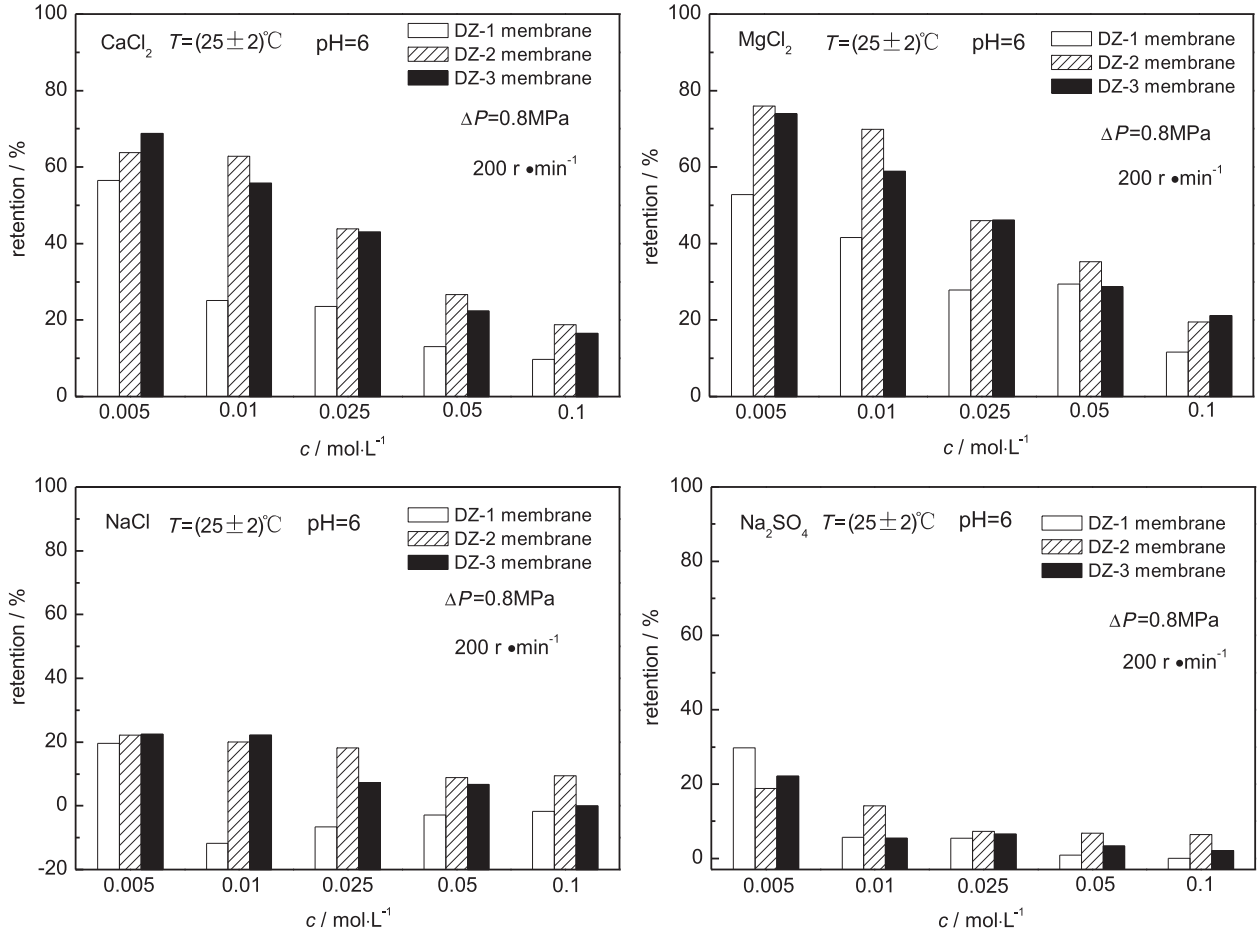


**Fig. 13.** Ionic retention of $ZrO_2$ membranes as a function of salt concentration.

sols with the average size larger than 8 nm show comparatively higher retention rates (in the range of 65%–75%) towards 0.005 mol·L$^{-1}$ divalent salt solutions (*i.e.* $CaCl_2$ and $MgCl_2$) and lower retention rates (<20%) towards 0.005 mol·L$^{-1}$ mono-valent salt solutions (*i.e.* NaCl and $Na_2SO_4$). The iso-electric point of zirconia membrane is estimated to be approximately at pH = 7.0 based on the relationship between solution pH and zeta potential value of zirconia membrane [36,41,42]. That is to say, the zirconia membrane surface is always positively charged in aqueous solutions with pH values lower than 7. Therefore, results displayed in Fig. 13 are reasonable based on the electrical interaction between membrane surface charge and ions [43]. The results also confirm that sols with an average size larger than the pore size of γ-$Al_2O_3$ support can efficiently prevent from intensive penetration into the support and, hence, lead to the formation of defect-free zirconia NF membranes.

The salt retention rates of DZ membranes as a function of trans-membrane pressure are shown in Fig. 14. Some membranes show a slight increase in the retention as pressure increases, while some show independent results. The results can be explained by diffusion (due to a concentration gradient), convection (due to a pressure gradient) and electromigration (due to an electrical potential gradient) mechanisms [35]. The DZ-1 membrane fabricated with DZ-1 sol with the average size (3.8 nm) slightly smaller than the pore size of γ-$Al_2O_3$ support exhibits retention rates towards $CaCl_2$ and $MgCl_2$ as low as 30% and 36%, respectively, while DZ-2 and DZ-3 membranes fabricated with 8.6 and 12 nm-sized sols, respectively, exhibit better nanofiltration performance towards 0.005 mol·L$^{-1}$ salt solutions, as evidenced by the retention rates of 64% ($CaCl_2$) and 76% ($MgCl_2$), and 55% ($CaCl_2$) and 62% ($MgCl_2$), respectively. The higher retention rates of DZ-2 membrane may be ascribed to a comparatively smaller pore size. Skluzacek *et al.* [38] and Tsuru *et al.* [44] have found that the membrane with smaller pore size holds higher charge density, resulting in higher retention rates towards salt solutions. It should be noted that the salt retention rates of DZ membranes are in the sequence of $R$(DZ-2) > $R$(DZ-3) > $R$(DZ-1), which is also consistent with the PEGs retention data.

The chemical stability of zirconia powder, represented by $Zr^{4+}$ concentration of the solution with zirconia powder corroded in different pH environments for 4 days, is depicted in Table 4. The variation of concentration of dissolved zirconia is not significant with corroded in a wide pH range of 1–12, while the increase of dissolved $Zr^{4+}$ is significant in a solution at pH of 13. Results indicate that the 400 °C-calcined zirconia powder is stable in a pH window of 1–12, which is a considerable improvement in comparison with γ-$Al_2O_3$ [25] and polymers [22] (Fig. 15).

**Table 4**
$Zr^{4+}$ concentration of the solution with zirconia powder corroded under different pH environment

| pH | 1 | 2 | 3 | 11 | 12 | 13 |
|---|---|---|---|---|---|---|
| Zr ion concentration/μg·L$^{-1}$ | 13 | <10 | <10 | 19 | 38 | 266 |

## 4. Conclusions

Zirconia membranes derived from sols with different particle size distributions were successfully fabricated *via* sol–gel processes. Effect of sol size on the NF performance of zirconia membranes were investigated in detail. Nitrogen adsorption–desorption results show that the

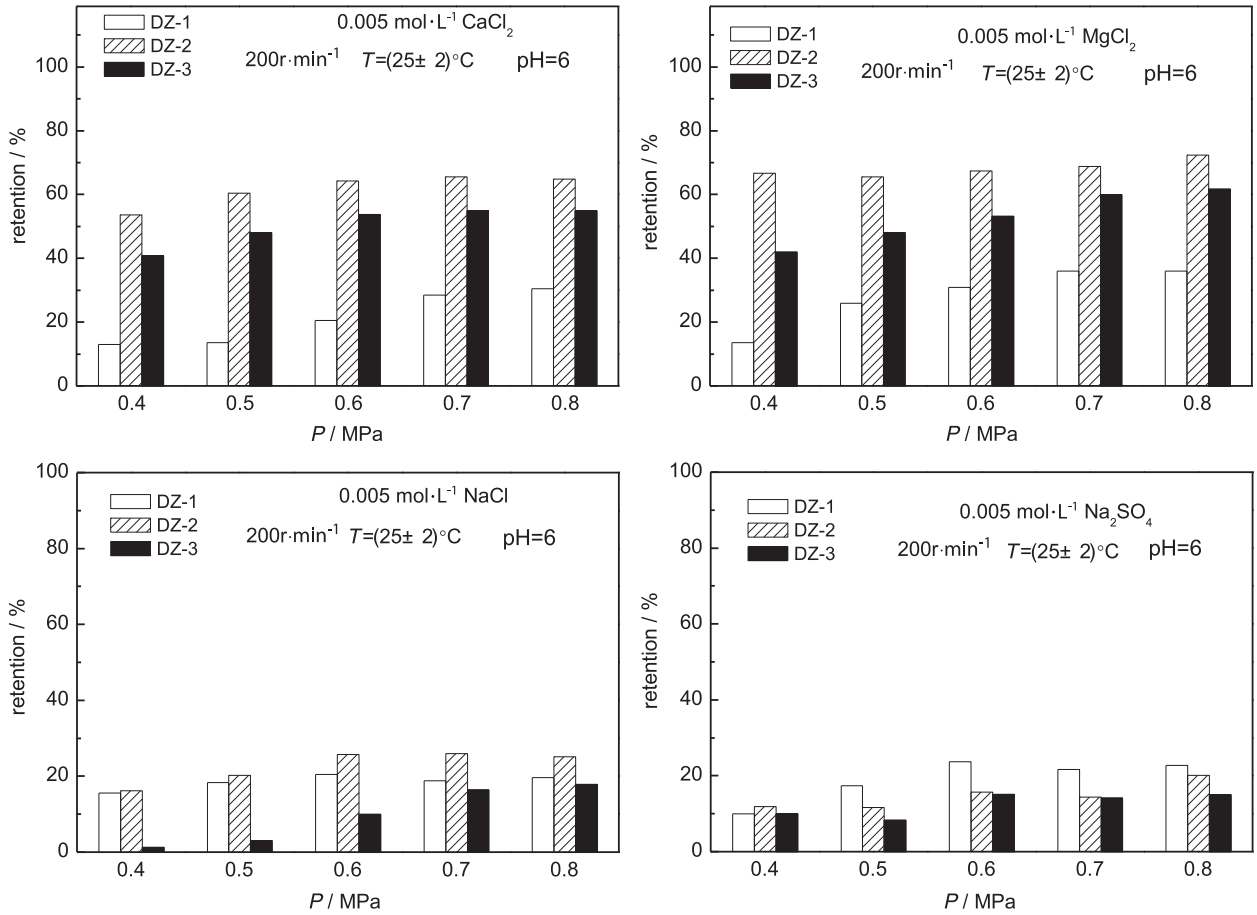


**Fig. 14.** Ionic retention of $ZrO_2$ membranes as a function of trans-membrane pressure.

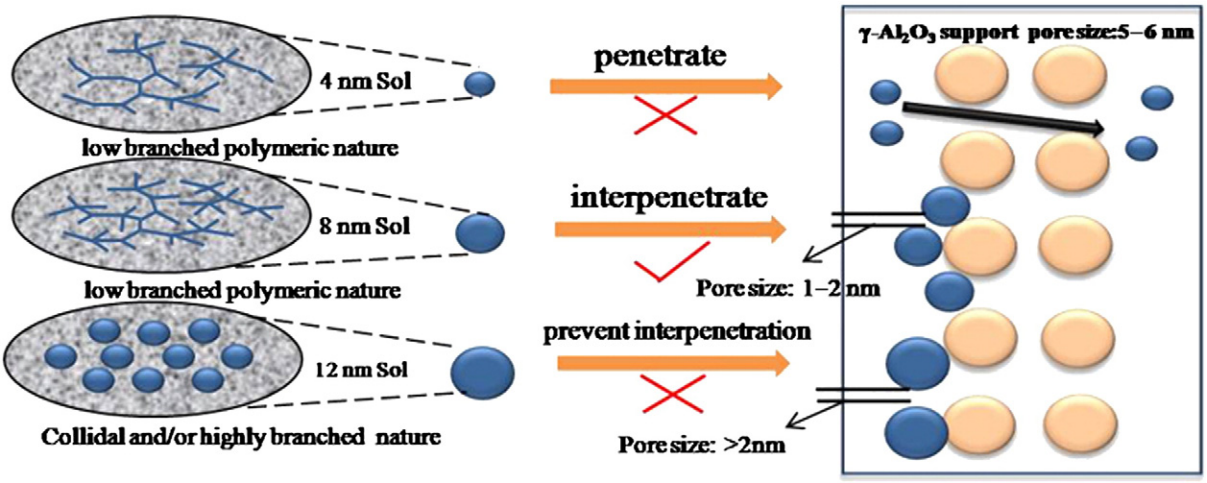


**Fig. 15.** The effect of sol size on nanofiltration performance of zirconia membrane.

increase of sol size, from 3.8 nm to 12 nm, increases porous volume and form preferred microporous structures from polymeric to colloidal in nature. FESEM analysis, MWCO and salt retention results show that the sol size is one of the key factors in obtaining a continuous and defect-free zirconia nanofiltration membrane, as also can be seen from Fig. 15. The zirconia sol with an average size larger than the pore size of $\gamma$-$Al_2O_3$ support can efficiently prevent from intensive penetration into the support and, forming a homogeneous zirconia membrane. The average size of zirconia sol should also be adjusted smaller than 12 nm. Under such condition, zirconia sols will prefer to retain a low branched polymeric nature and allow interpenetration of polymer chains. A microporous zirconia membrane fabricated by dip-coating zirconia sol with an appropriate average size of 8.6 nm shows a MWCO value of 1195 and high retention rates towards $CaCl_2$ (64%) and $MgCl_2$ (76%). The material is chemically stable in a wide pH window of 1–12.

## Nomenclature

| | |
|---|---|
| MWCO | the molecular weight cut-off, Da |
| *R* | the pore radius of membrane, nm |

## References


[1] P. Vandezande, L.E.M. Gevers, I.F.J. Vankelecom, Solvent resistant nanofiltration: separating on a molecular level, *Chem. Soc. Rev.* 37 (2) (2008) 365–405.
[2] A. Buekenhoudt, A. Kovalevsky, I.J. Luyten, F. Snijkers, Basic Aspects in Inorganic Membrane Preparation, Comprehensive Membrane Science and Engineering, Elsevier, Amsterdam, 2008, pp. 217–252.
[3] G.M. Rios, R. Joulie, S.J. Sarrade, M. Carlès, Investigation of ion separation by microporous nanofiltration membranes, *AIChE J.* 42 (9) (1996) 2521–2528.
[4] T. Tsuru, T. Nakasuji, M. Oka, M. Kanezashi, T. Yoshioka, Preparation of hydrophobic nanoporous methylated $SiO_2$ membranes and application to nanofiltration of hexane solutions, *J. Membr. Sci.* 384 (1–2) (2011) 149–156.
[5] J. Sekulic, J.E. ten Elshof, D.H.A. Blank, A microporous titania membrane for nanofiltration and pervaporation, *Adv. Mater.* 16 (17) (2004) 1546–1550.
[6] A. Julbe, C. Guizard, A. Larbot, L. Cot, A. Giroir-Fendlerb, The sol–gel approach to prepare candidate microporous inorganic membranes for membrane reactors, *J. Membr. Sci.* 77 (1993) 137–153.
[7] P. Blanc, A. Larbot, J. Palmeri, M. Lopez, L. Cot, Hafnia ceramic nanofiltration membranes. Part I. Preparation and characterization, *J. Membr. Sci.* 149 (2) (1998) 151–161.
[8] C. Guizard, Sol–gel chemistry and its application to porous membrane processing, Fundamentals of Inorganic Membrane Science and Technology, Elsevier, Amsterdam, 1996, pp. 227–258.
[9] J. Sekulic, J.E. ten Elshof, D.H.A. Blank, Synthesis and characterization of microporous titania membranes, *J. Sol-Gel Sci. Technol.* 31 (1) (2004) 201–204.
[10] C.S.W. Jeffrey, L.C. Wu, An improved synthesis of ultrafiltration zirconia membranes via the sol–gel route using alkoxide precursor, *J. Membr. Sci.* 167 (2000) 253–261.
[11] H.L. Castricum, A. Sah, R. Kreiter, D.H.A. Blank, J.F. Vente, J.E. ten Elshof, Hydrothermally stable molecular separation membranes from organically linked silica, *J. Mater. Chem.* 18 (18) (2008) 2150–2158.
[12] H.L. Castricum, R. Kreiter, H.M. van Veen, D.H.A. Blank, J.F. Vente, J.E. ten Elshof, High-performance hybrid pervaporation membranes with superior hydrothermal and acid stability, *J. Membr. Sci.* 324 (1–2) (2008) 111–118.
[13] R. Kreiter, M. Rietkerk, B. Bonekamp, H. van Veen, V. Kessler, J. Vente, Sol–gel routes for microporous zirconia and titania membranes, *J. Sol-Gel Sci. Technol.* 48 (1) (2008) 203–211.
[14] T. Van Gestel, D. Sebold, H. Kruidhof, H.J.M. Bouwmeester, $ZrO_2$ and $TiO_2$ membranes for nanofiltration and pervaporation. Part 2. Development of $ZrO_2$ and $TiO_2$ toplayers for pervaporation, *J. Membr. Sci.* 318 (1–2) (2008) 413–421.
[15] T. Van Gestel, H. Kruidhof, D.H.A. Blank, H.J.M. Bouwmeester, $ZrO_2$ and $TiO_2$ membranes for nanofiltration and pervaporation Part 1. Preparation and characterization of a corrosion-resistant $ZrO_2$ nanofiltration membrane with a MWCO < 300, *J. Membr. Sci.* 284 (1–2) (2006) 128–136.
[16] T. Tsuru, S.-I. Wada, S. Izumi, M. Asaeda, Silica–zirconia membranes for nanofiltration, *J. Membr. Sci.* 149 (1) (1998) 127–135.
[17] H.L. Castricum, G.G. Paradis, M.C. Mittelmeijer-Hazeleger, R. Kreiter, J.F. Vente, J.E. ten Elshof, Tailoring the separation behavior of hybrid organosilica membranes by adjusting the structure of the organic bridging group, *Adv. Funct. Mater.* 21 (12) (2011) 2319–2329.
[18] H.L. Castricum, A. Sah, J.A.J. Geenevasen, R. Kreiter, D.H.A. Blank, J.F. Vente, J.E. Elshof, Structure of hybrid organic–inorganic sols for the preparation of hydrothermally stable membranes, *J. Sol-Gel Sci. Technol.* 48 (1–2) (2008) 11–17.
[19] R. Kreiter, M.D.A. Rietkerk, H.L. Castricum, H.M. Veen, J.E. ten Elshof, J.F. Vente, Evaluation of hybrid silica sols for stable microporous membranes using high-throughput screening, *J. Sol-Gel Sci. Technol.* 57 (3) (2010) 245–252.
[20] M. Janssen, C. Müller, D. Vogt, 'Click' dendritic phosphines: Design, synthesis, application in Suzuki coupling, and recycling by nanofiltration, *Adv. Synth. Catal.* 351 (3) (2009) 313–318.
[21] I. Voigt, M. Stahn, St. Wöhner, A. Junghans, J. Rost, W. Voigt, Integrated cleaning of coloured waste water by ceramic NF membranes, *Sep. Purif. Technol.* 25 (1–3) (2001) 509–512.
[22] F.N. Liu, G.L. Zhang, Q. Meng, H.Z. Zhang, Performance of nanofiltration and reverse osmosis membranes in metal effluent treatment, *Chin. J. Chem. Eng.* 16 (3) (2008) 441–445.
[23] G. Yang, H. Shi, W.Q. Liu, W.H. Xing, N.P. Xu, Investigation of $Mg^{2+}/Li^{+}$ separation by nanofiltration, *Chin. J. Chem. Eng.* 19 (4) (2011) 586–589.
[24] H. Qi, G.Z. Zhu, L. Li, N.P. Xu, Fabrication of a sol–gel derived microporous zirconia membrane for nanofiltration, *J. Sol-Gel Sci. Technol.* 62 (2012) 208–216.
[25] T. Van Gestel, C. Vandecasteele, A. Buekenhoudt, C. Dotremont, J. Luyten, R. Leysen, B. Van der Bruggen, G. Maes, Alumina and titania multilayer membranes for nanofiltration: preparation, characterization and chemical stability, *J. Membr. Sci.* 207 (1) (2002) 73–89.
[26] U. Aust, S. Benfer, M. Dietze, A. Rost, G. Tomandl, Development of microporous õceramic membranes in the system $TiO_2/ZrO_2$, *J. Membr. Sci.* 281 (2006) 463–471.
[27] S. Naci Koç, Zirconium titanate synthesis by diethanol amine based sol–gel route, *J. Sol-Gel Sci. Technol.* 38 (3) (2006) 277–281.
[28] G.I. Spijksma, D.H.A. Blank, H.J.M. Bouwmeester, V.G. Kessler, Modification of different zirconium propoxide precursors by diethanolamine. Is there a shelf stability issue for sol–gel applications? *Int. J. Mol. Sci.* 10 (11) (2009) 4977–4989.
[29] C.-H. Chang, R. Gopalanm, Y.S. Lin, A comparative study on thermal and hydrothermal stability of alumina, titania and zirconia membranes, *J. Membr. Sci.* 91 (1994) 27–45.
[30] J. Sekulić, A. Magraso, J.E. ten Elshof, D.H.A. Blank, Influence of $ZrO_2$ addition on microstructure and liquid permeability of mesoporous $TiO_2$ membranes, *Microporous Mesoporous Mater.* 72 (1–3) (2004) 49–57.
[31] H. Zou, Y.S. Lin, Structural and surface chemical properties of sol–gel derived $TiO_2$–$ZrO_2$ oxides, *Appl. Catal. A* 265 (1) (2004) 35–42.
[32] A. Díaz-Parralejo, A. Macías-García, E.M. Cuerda-Correa, R. Caruso, Influence of the type of solvent on the textural evolution of yttria stabilized zirconia powders obtained by the sol–gel method: characterization and study of the fractal dimension, *J. Non-Cryst. Solids* 351 (24–26) (2005) 2115–2121.

[33] G. Vanderdonk, J. Serra, W. Meulenberg, Microporous and mesoporous 8YSZ materials derived from polymeric acetylacetone-modified precursors for inorganic membrane applications, *J. Non-Cryst. Solids* 354 (31) (2008) 3723–3731.
[34] F.D. Monte, W. Larsen, J.D. Mackenzie, Stabilization of tetragonal $ZrO_2$ in $ZrO_2$–$SiO_2$ binary oxides, *J. Am. Ceram. Soc.* 83 (3) (2000) 628–634.
[35] P. Puhlfürß, A. Voigt, R. Weber, M. Morbéb, Microporous $TiO_2$ membranes with a cut off <500 Da, *J. Membr. Sci.* 174 (2000) 123–133.
[36] R. Vacassy, C. Guizard, V. Thoraval, L. Cot, Synthesis and characterization of microporous zirconia powders: application in nanofilters and nanofiltration characteristics, *J. Membr. Sci.* 132 (1997) 109–118.
[37] Q. Xu, M.A. Anderson, Sol–gel route to synthesis of microporous ceramic membranes: preparation and characterization of microporous $TiO_2$ and $ZrO_2$ xerogels, *J. Am. Ceram. Soc.* 77 (7) (1994) 1939–1945.
[38] J. Skluzacek, M. Tejedor, M. Anderson, NaCl rejection by an inorganic nanofiltration membrane in relation to its central pore potential, *J. Membr. Sci.* 289 (1–2) (2007) 32–39.
[39] J. Schaep, C. Vandecasteele, B. Peeters, J. Luyten, C. Dotremont, D. Roels, Characteristics and retention properties of a mesoporous γ-$Al_2O_3$ membrane for nanofiltration, *J. Membr. Sci.* 163 (1999) 229–237.
[40] G.T. Ballet, A. Hafiane, M. Dhahbi, Influence of operating conditions on the retention of phosphate in water by nanofiltration, *J. Membr. Sci.* 290 (1–2) (2007) 164–172.
[41] T. Tsuru, H. Takezoe, M. Asaeda, Ion separation by porous silica–zirconia nanofiltration membranes, *AIChE J* 44 (3) (1998) 765–768.
[42] J.N. Ryan, M. Elimelech, J.L. Baeseman, R.D. Magelk, Silica-coated titania and zirconia colloids for subsurface transport field experiments, *Environ. Sci. Technol.* 34 (2000) 2000–2005.
[43] W.Q. Jin, N.P. Xu, J. Shi, Progress in inorganic nanofiltration membranes, *Chin. J. Chem. Eng.* 6 (1) (1998) 59–67.
[44] T. Tsuru, T. Yoshioka, M. Asaeda, Titania membranes for liquid phase separation effect of surface charge on flux, *Sep. Purif. Technol.* 25 (2001) 307–314.